JCTC Journal of Chemical Theory and Computation

Electrostatic Interactions in Dissipative Particle Dynamics: Toward a Mesoscale Modeling of the Polyelectrolyte Brushes

Cyrille Ibergay,[†] Patrice Malfreyt,*[,†] and Dominic J. Tildesley[‡]

Laboratoire de Thermodynamique et Interactions Moléculaires, FRE CNRS 3099, Université Blaise Pascal, 63177 Aubière Cedex, France, and Unilever Research, Port Sunlight, Bebington, Wirral CH63 3JW, U.K.

Received June 9, 2009

Abstract: We report mesoscopic simulations of bulk electrolytes and polyelectrolyte brushes using the dissipative particle dynamics (DPD) method. The calculation of the electrostatic interactions is carried out using both the Ewald summation method and the particle−particle particle-mesh technique with charges distributed over the particles. The local components of the pressure tensor are calculated using the Irving and Kirkwood, and the method of planes and mechanical equilibrium is demonstrated. The profiles of the normal component of the pressure tensor are shown to be similar for both the Ewald and particle−particle particle-mesh methods for a single polyelectrolyte brush. We show that the PPPM method with the MOP technique is the appropriate choice for simulations of this type. The mesoscale modeling of a strongly stretched polylectrolyte brush formed by strong charged polymer chains at a high grafting density shows that the polyelectrolyte follows the nonlinear osmotic regime, as expected from the calculation of the Gouy−Chapman length and the dimensionless Manning ratio.

1. Introduction

Molecular simulations of polymers and surfactant solutions demands modeling on a hierarchy of length and time scales spanning several orders of magnitude. For example, in a polymer brush, the size of the atomic constituents is on the order of 1 Å, and the fastest motions are at times on the order of 10^{-14} s, whereas collective relaxation in the system can occur on a scale of micrometers and at times that exceed 1 ms. Molecular simulations of brushes require that the equations of motion be solved with a time scale of a femtosecond and a length scale of angströms, and this might not be the most efficient approach for studying mesoscale phenomena such as the friction between brushes.

The development of simulation techniques capable of accessing mesoscopic length and time scales is an area of active research.[1−4] One approach is the dissipative particle dynamics (DPD) method, initially proposed by Hoogerbrugge and Koelman.[1] This method consists of reducing the complexity of the atomistic description of the system through the use of a coarse-grained model. In this method, a number of atoms are combined into particles that interact with each other through soft conservative and pairwise dissipative and random forces. The dissipative and random forces are related through the fluctuation−dissipation theorem, leading to a local conservation of the momentum, which is required for a correct description of hydrodynamics.[3] DPD has been successfully applied to investigate a variety of soft-matter problems such as the microphase separation of block copolymers,[5,6] polymer surfactants in solution,[7] and the structure and rheology of biological membranes.[8]

We have used the DPD approach to study the interaction between two solid surfaces coated with grafted polymer chains. At a relatively high surface coverage under good solvent conditions, the polymer chains are strongly stretched in the direction perpendicular to the surface; this leads to a structure called a polymer brush. End-grafted polymer chains give rise to a wide range of important industrial applications

* Corresponding author e-mail: Patrice.MALFREYT@univ-bpclermont.fr.

[†] TIM, FRE CNRS 3099.

[‡] Unilever Research.

10.1021/ct900296s CCC: $40.75
Published on Web 10/29/2009

in the stabilization of colloidal suspensions, adhesion, lubrication, friction, and wear. We have also adapted the standard DPD method[9] to model the friction between two polymer brushes as a function of the quality of the solvent[10] and the separation between the surfaces.[11,12]

In this article, we aim to simulate charged polymers grafted to surfaces. Recent experiments have shown that polyelectrolyte brushes are better lubricants than neutral brushes.[13] However, the inclusion of the long-range electrostatic interactions in DPD is required to model such effects accurately. Electrostatic interactions were recently introduced into DPD by Groot[14] and by Alejandre and co-workers.[15] Both proposed replacing the point charge at the center of the DPD particle with a charge distribution smeared across the particle. Groot proposed a method in which the electrostatic field is calculated locally using a grid technique, whereas Alejandre et al. used a modification of the standard Ewald sum method.[16] These two methods have been applied to study a bulk electrolyte and polyelectrolyte−surfactant solutions.[14,15] Good agreement was found between the two methods for the radial distribution functions of charged particles in bulk electrolytes and polyelectrolyte−surfactant solutions. In this article, we compare these methods for systems with reduced periodicity.

In a brush system, the calculation of the friction coefficient requires the calculation of the normal and tangential components of the pressure tensor. When the system is nonperiodic in one dimension, it is important to calculate profiles of the pressure tensor along this axis. This establishes the mechanical equilibrium in the system and allows an accurate average value of the friction to be obtained from the profile.[10,12,17] In this work, we consider the most efficient way of calculating the profiles of the pressure tensor when electrostatic interactions are included in the DPD approach.

Different methods can be used to calculate the local pressure components along a specific direction. The potential term in the pressure tensor introduces arbitrariness because there is a choice of the contour joining the two particles. Several choices have been developed to calculate the potential component of the pressure tensor, including those of Irving and Kirkwood (IK)[18] and Harasima.[19] The IK definition is applicable only for pairwise-additive interactions. Contributions such as the reciprocal part of the electrostatic interactions treated with the Ewald sum are not pairwise-additive, so the definition of Harasima can be used.[20,21] An alternative approach consists of using the method of planes (MOP) formalism,[22] which avoids the heuristic notions of the force across a unit area. This method can be applied to both pairwise-additive and non-pairwise-additive interactions. In this work, we compare these approaches.

Additionally, in some important cases, the modeling of a surface requires a system that is nonperiodic in the third dimension. The conventional Ewald summation method can be applied by elongating the primary cell in the direction of the surface by adding a sufficiently large vacuum between the periodic images. The aim is to dampen out the interslab interactions. This methodology is often referred to as the supercell approximation, and it has been applied successfully.[23−25] To remove the forces due to the net dipole of the periodically repeating slabs, a correction dipole term must be added.[23,24] This methodology is known as the EW3DC method.

There are some quasi-periodic Ewald methods, such those due to Hautman and Klein[26] and Lekner,[27] that can be applied in these geometries. These often result in series expansions of the electrostatic interactions where the convergence depends on the particular distribution of particles. In addition, these methods can be extremely expensive in terms of computational resources. However, the MMM technique[28] adapted by Strebel and Sperb[29] for slab geometries[30,31] maintains a reasonable computational cost with an $O(N^{5/3} \log N)$ behavior, where N is the number of charged particles. Therefore, we do not consider these methods further in the work. Instead, we employ the Groot particle−particle particle-mesh (PPPM) method in the case of a slab geometry, as well as the EW3DC approach.

To explore the different methods for accounting for the electrostatic interactions in the calculation of the local pressure components, we focus on three model systems: a three-dimensional bulk electrolyte, a bulk electrolyte embedded between two parallel surfaces, and a system of charged polyelectrolyte brushes. We then use these systems to validate the methodology, and we complete this work with a preliminary study of grafted polyelectrolytes, which represent an interesting topic with many unresolved problems for both experiment and theory. The system studied presently is a model system formed with a high surface coverage and a relatively strong charge fraction.

In section 2, we present the conventional forces used in the DPD model. In section 3, we describe the two techniques used for the calculation of the electrostatic forces. The different definitions for the calculation of the local components of the pressure tensor are described in section 4. The results for the different model systems are given in section 5. Finally, we conclude in section 6 by providing a brief summary of our main results.

2. Dissipative Particle Dynamics (DPD) Model

2.1. Standard DPD Forces. In the DPD approach, solvent particles are coarse-grained into soft beads that interact with the pairwise-additive force $\mathbf{f}_i$ defined as the sum of three contributions

$$\mathbf{f}_i = \sum_{j \neq i} (\mathbf{f}_{ij}^{\mathrm{C}} + \mathbf{f}_{ij}^{\mathrm{R}} + \mathbf{f}_{ij}^{\mathrm{D}}) \tag{1}$$

where $\mathbf{f}_{ij}^{\mathrm{C}}$, $\mathbf{f}_{ij}^{\mathrm{R}}$, and $\mathbf{f}_{ij}^{\mathrm{D}}$ are the conservative, random, and dissipative forces, respectively. The conservative repulsive force, $\mathbf{f}_{ij}^{\mathrm{C}}$, derives from a soft interaction potential and is expressed as

$$\mathbf{f}_{ij}^{\mathrm{C}} = \begin{cases} a_{ij}\omega^{\mathrm{C}}(r_{ij})\hat{\mathbf{r}}_{ij} & (r_{ij} < r_{\mathrm{c}}) \\ 0 & (r_{ij} \geq r_{\mathrm{c}}) \end{cases} \tag{2}$$

where a_{ij} is the maximum repulsion parameter between particles i and j, r_{ij} is the relative displacement of particles i and j, and $\hat{\mathbf{r}}_{ij}$ is the corresponding unit vector. The weight function $\omega^{\mathrm{C}}(r_{ij})$ is equal to $1 - r_{ij}/r_{\mathrm{c}}$ for $r_{ij} \leq r_{\mathrm{c}}$ and vanishes

for $r_{ij} \geq r_c$. The dissipative and random forces are given by

$$\mathbf{f}_{ij}^{D} = -\gamma\omega^{D}(r_{ij})(\hat{\mathbf{r}}_{ij} \cdot \mathbf{v}_{ij})\hat{\mathbf{r}}_{ij} \quad (3)$$

$$\mathbf{f}_{ij}^{R} = \sigma\omega^{R}(r_{ij})\theta_{ij}\frac{1}{\sqrt{\delta t}}\hat{\mathbf{r}}_{ij} \quad (4)$$

where δt is the time step. $\mathbf{v}_{ij} = \mathbf{v}_i - \mathbf{v}_j$ is the relative velocity, σ is the amplitude of the noise, θ_{ij} is a random Gaussian number with zero mean and unit variance. γ and σ are the dissipation strength and noise strength, respectively. The terms $\omega^{D}(r_{ij})$ and $\omega^{R}(r_{ij})$ are dimensionless weighting functions. Espanol and Warren[3] showed that the system will sample the canonical ensemble and obey the fluctuation−dissipation theorem if the following conditions are satisfied:

$$\gamma = \frac{\sigma^2}{2k_B T} \quad \text{and} \quad \omega^{D}(r_{ij}) = [\omega^{R}(r_{ij})]^2 \quad (5)$$

where k_B is the Boltzmann constant and T is the temperature. The weighting function $\omega^{R}(r_{ij})$ is chosen to be similar to $\omega^{C}(r_{ij})$.

The equations of motion are integrated using a modified version of the velocity-Verlet algorithm.[14] The force is updated once per iteration, and because the force depends on the velocities, the velocity in the next time step has to be estimated by a predictor algorithm. The velocity is then corrected in the last step. The reduced time step δt was taken as 0.02 for all of the simulations, except for those involving polyelectrolyte brushes, for which it was equal to 0.06.

When fully flexible polymer chains are considered in solvent, the integrity of the polymer chain is ensured by an additional spring force between neighboring beads given by

$$\mathbf{f}_{ij}^{S} = -k_s(\mathbf{r}_{ij} - r_0)\hat{\mathbf{r}}_{ij} \quad (6)$$

where the equilibrium bond distance r_0 is 0 and the spring constant $k_s = 4.0$. This pairwise force is then added to the sum of the DPD conservative force in eq 1.

3. Electrostatic Interactions

In the following sections, we present two techniques to take into account the electrostatic interactions at a mesoscopic level. The first one consists of solving the electrostatic field on a grid. This is referred to as the particle−particle particle-mesh (PPPM) algorithm,[32−34] although, in the original version of the PPPM algorithm, the far field was solved using a fast Fourier transform.[14,32,35] The second consists of adapting the standard Ewald method to DPD particles.

3.1. Particle−Particle Particle-Mesh (PPPM) Method. Electrostatic interactions were incorporated into the DPD model by Groot.[14] The first step consists of finding a model for the density distribution adapted to a charged bead. The use of a soft potential in DPD allows for the overlap between DPD beads. When charged DPD beads are modeled, this can lead to the formation of artificial ion pairs and cause the divergence of the electrostatic potential. To avoid this problem, Groot chose to spread out the charges using the distribution

$$f(r) = \frac{3}{\pi r_e^3}(1 - r/r_e) \quad \text{for} \quad r < r_e \quad (7)$$

where r_e is the electrostatic smearing radius and $f(r) = 0$ when r is greater than r_e. The expression for the potential between two of these charge clouds is given in Appendix A, and the representation of the potential and its corresponding force with respect to the distance is shown in Figure 1. The electrostatic field is then solved on a lattice according to the method of Beckers et al.[32] The charges are assigned to the lattice nodes within the cell, and the long-range part of the interaction potential is calculated by solving the Poisson equation on the grid. Details of the charge assignment can be found in Groot's[14] original article. Whereas, in the original PPPM method, the far field was solved using a Fourier transform, the method developed by Groot used real-space successive overdamped relaxations. This makes the Groot method close to the multigrid method of Sagui and Darden.[34] However, for convenience, this method will be referred to as the PPPM method in the present work.

The electrostatic force $\mathbf{f}_i^{E}$ on a charged bead i is calculated from

$$\mathbf{f}_i^{E}(\mathbf{r}_i) = -q_i \sum_j f_j(\mathbf{r}_i)\nabla\psi(\mathbf{r}_j) \quad (8)$$

where $\mathbf{r}_i$ is the position of the charged bead i and q_i is the number of unit charges on bead i. $f_j(\mathbf{r}_i)$ is defined as

$$f_j(\mathbf{r}_i) = \frac{1 - |\mathbf{r}_j - \mathbf{r}_i|/r_e}{\sum_n (1 - |\mathbf{r}_n - \mathbf{r}_i|/r_e)} \quad (9)$$

where $\mathbf{r}_j$ is the position of the node j and the sum over n runs over all nodes within a distance r_e from $\mathbf{r}_i$. This function means that a charge proportional to $f(r)$ in eq 7 is assigned to each node i and normalized such that the sum of all of the charges within a distance r_e equals the charge on the bead i. $\psi(\mathbf{r}_j)$ is the local electrostatic field at lattice node j.

The field $\psi(\mathbf{r}_j)$ is calculated from the Poisson equation expressed in reduced DPD units as

$$\nabla^* \cdot [p(r)\nabla^*\psi] = -\Gamma\rho^* \quad (10)$$

where ρ^* is the concentration of cations minus the concentration of anions per r_c^3, ∇^* is the gradient in reduced units, and $p(r)$ is the local polarizability relative to that of pure water.

The total momentum of the simulation cell is conserved by removing a possible residual force for each charge. This residual force is on the order of 5×10^{-5} in reduced units and is expressed as $\sum_i^N q_i \mathbf{f}_i^{E}/N$. The total force $\mathbf{f}_i$ of eq 1 is then modified by adding the $\mathbf{f}_i^{E}$ contribution and the residual force.

3.2. Ewald Summation (EW3DC) Method. The method recently proposed by González-Melchor et al.[15] consists of combining the Ewald technique[16] and a charge distribution for particles. In the case of an electroneutral system formed by N particles, with each particle i carrying a point charge q_i at position r_i in a volume $V = L_x L_y L_z$, the long-

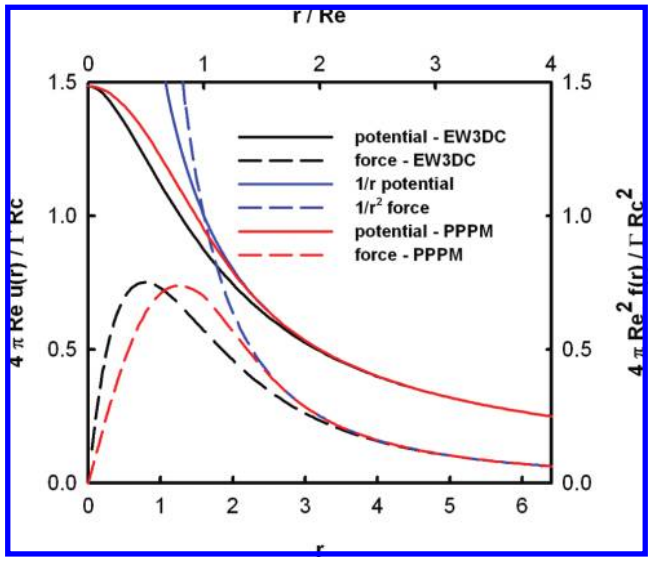

Figure 1. Electrostatic potential and force calculated by the EW3DC and PPPM methods. For comparison, we include the Coulombic potential and force, which diverges at $r = 0$. The x axis is expressed in standard DPD units (r/r_c), whereas the top axis gives the distance r/r_e. The potential and force expressions are plotted for two equal-sign charge distributions.

range electrostatic interactions are decomposed into contributions in real space and in reciprocal space

$$U(\mathbf{r}^N) = \frac{1}{4\pi\varepsilon_0\varepsilon_r}\left[\sum_i \sum_{j>i} q_i q_j \frac{\mathrm{erfc}(\alpha r_{ij})}{r_{ij}} + \frac{2\pi}{V}\sum_{k\neq 0}^{\infty} Q(h)\, S(\mathbf{h})\, S(-\mathbf{h}) - \frac{\alpha}{\sqrt{\pi}}\sum_i^N q_i^2\right] \quad (11)$$

where erfc(x) is the complementary error function. α is chosen so that only pair interactions in the central cell need to be considered in evaluating the first term of eq 11. The functions $Q(h)$ and $S(\mathbf{h})$ are defined by the equations

$$Q(h) = \exp(-h^2/4\alpha^2)/h^2 \quad (12)$$

$$S(\mathbf{h}) = \sum_{i=1}^{N} q_i \exp(i\mathbf{h}\cdot\mathbf{r}_i) \quad (13)$$

where the components of the reciprocal vector $\mathbf{h}$ are defined as $2\pi(l/L_x, m/L_y, n/L_z)$ where l, m, and n take values of 0, ±1, ±2, ..., $\pm\infty$.

To remove the divergency of the Coulombic potential at $r = 0$, Alejandre and co-workers[15] considered a Slater-type charge distribution on DPD particles of the form

$$f(r) = \frac{q}{\pi\lambda^3}\exp(-2r/\lambda) \quad (14)$$

where λ is the decay length of the charge. The distribution is normalized to q.

The magnitude of the reduced force between two charge distribution is then given by the sum of a pairwise-additive contribution $\mathbf{f}_{ij}^{E,R}$ coming from the real-space term and a non-pairwise-additive contribution $\mathbf{f}_i^{E,K}$ from the reciprocal-space term. These two contributions are given by the expressions

$$\mathbf{f}_{ij}^{E,R} = \frac{\Gamma}{4\pi} q_i q_j \left[\frac{2}{\sqrt{\pi}}\exp(-\alpha^2 r_{ij}^2) + \mathrm{erfc}(\alpha r_{ij})\right] \times \{[1 - \exp(-2\beta r_{ij})][1 + 2\beta r_{ij}(1 + \beta r_{ij})]\}\frac{\mathbf{r}_{ij}}{r_{ij}^3} \quad (15)$$

$$\mathbf{f}_i^{E,K} = -\frac{\Gamma}{4\pi} q_i \left\{\frac{2\pi}{V}\sum_{\mathbf{h}\neq 0} Q(h)\mathbf{h} \times \mathrm{Im}[\exp(-i\mathbf{h}\cdot\mathbf{r}_i)\, S(\mathbf{h})]\right\} \quad (16)$$

where Im denotes the imaginary part of the complex variable.

To remove the net dipole moment of the simulation cell, a z-component force is added for each bead

$$\mathbf{f}_{i,z} = -\frac{\Gamma}{V} M_z \quad (17)$$

where M_z is the net dipole moment of the simulation cell given by $\sum_i q_i \mathbf{r}_i$ and V is the volume expressed in reduced units. This contribution is the correction term from Yeh and Berkowitz,[23] which results from the plane-wise summation method proposed by Smith.[36]

Within the EW3DC method, the force acting on the ith particle becomes

$$\mathbf{f}_i = \mathbf{f}_i^{E,K} + \mathbf{f}_{i,z} + \sum_{j\neq i}(\mathbf{f}_{ij}^{C} + \mathbf{f}_{ij}^{R} + \mathbf{f}_{ij}^{D} + \mathbf{f}_{ij}^{E,R}) \quad (18)$$

The pairwise $\mathbf{f}_{ij}^{E,R}$ force is then added to sum of the conservative, dissipative, and random pairwise forces, whereas $\mathbf{f}_i^{E,K}$ and $\mathbf{f}_{i,z}$, which are not pairwise-additive, are added to the force $\mathbf{f}_i$ acting on particle i. The real parts of the force and energy equations are shown in Figure 1. In this work, we compare the results from these two different techniques, and it is worth pointing out that the potentials and forces are slightly different, as can be seen in Figure 1. In Groot's method, an approximate potential is derived from the distribution of eq 7. In Alejandre et al.'s method, the potential is exactly defined from eq 14. Following Alejandre et al., λ, the decay length of the charge, is adjusted to bring the potential into the closest possible agreement.

4. Calculation of the Pressure Tensor

4.1. Irving and Kirkwood (IK) Definition. The method of Irving and Kirkwood[18] (IK) is based on the notion of the force across a unit area. The pressure tensor is then written as a sum of a kinetic term and a potential term resulting from the intermolecular forces. Whereas the first term is well-defined, the potential term is subjected to arbitrariness because there is no unique way to determine which intermolecular forces contribute to the stress across dA. There are many ways of choosing the contour joining two interacting particles. Irving and Kirkwood[18] chose as a contour the straight line between the two particles. Other choices are possible and result from the lack of uniqueness in the definition of the microscopic stress tensor. The components of the pressure tensor[37−39] in the Irving and Kirkwood definition are expressed by

$$p_{\alpha\beta}(z) = \frac{1}{V}\left\langle \sum_{i=1}^{N} H(z_i) m_i \mathbf{v}_{i,\alpha}\mathbf{v}_{i,\beta} \right\rangle + \frac{1}{A}\left\langle \sum_{i=1}^{N-1}\sum_{j>i}^{N} (\mathbf{r}_{ij})_\alpha (\mathbf{f}_{ij})_\beta \frac{1}{|z_{ij}|}\ \theta\left(\frac{z - z_i}{z_{ij}}\right)\theta\left(\frac{z_j - z}{z_{ij}}\right)\right\rangle \quad (19)$$

The first term on the right-hand side of this equation represents the kinetic part, and the second term is the configurational pressure calculated from the conservative potentials. $H(z_i)$ is a top-hat function. α and β represent the x, y, and z directions. $\theta(x)$ is the unit step function defined by $\theta(x) = 0$ when $x < 0$ and $\theta(x) = 1$ when $x \geq 0$. A is the surface area normal to the z axis. The distance z_{ij} between two particles is divided into N_s slabs of thickness δz. Following Irving and Kirkwood, particles i and j give a local contribution to the pressure tensor in a given slab if the line joining these crosses, starts in, or finishes in the slab. Each slab has $1/N_s$ of the total contribution from the $i-j$ interaction. The normal component $p_N(z_k)$ is equal to $p_{zz}(z_k)$. $\mathbf{f}_{ij}$ in eq 19 is the pairwise force between particles i and j and sums the conservative, dissipative, random, and bead−spring forces, as well as the real-space contribution of the electrostatic forces. The reciprocal contribution to the electrostatic force is taken into account using the Harasima definition[19] of the pressure. The expressions for the local contributions to the pressure tensor are given in Appendix B for completeness.

4.2. Method of Planes (MOP) Definition. The method of planes[22] (MOP), introduced by Todd, Evans, and Daivis, is designed to calculate average cross-sectional pressures. The total pressure sums the kinetic and potential contributions as

$$p_{\alpha z}(z) = \frac{1}{A}\sum_{i=1}^{N}\left\langle \frac{m_i \mathbf{v}_{\alpha,i}\,\mathrm{sgn}(v_{i,z})}{\delta t}\right\rangle + \frac{1}{2A}\left\langle \sum_{i=1}^{N} \mathbf{f}_{\alpha,i}\,\mathrm{sgn}(z_i - z)\right\rangle \quad (20)$$

where $\mathbf{v}_{\alpha,i}$ is the α component of the velocity of particle i and $\mathbf{f}_{\alpha,i}$ is the α component of the total force on particle i. The kinetic part is due to the momentum of the molecules as they cross the area during Δt. If, between times t and $t + \Delta t$, particle i moves through planes, we use the sign of the z component of the velocity to specify the direction of the crossing. This method allows for the use of the total force $\mathbf{f}_{\alpha,i}$ calculated either from the PPPM or EW3DC method.

When the total force $\mathbf{f}_{\alpha,i}$ can be decomposed into pairwise contributions $\mathbf{f}_{\alpha,ij}$, the second term of eq 20 can be written as

$$\frac{1}{A}\left\langle \sum_{i}^{N-1}\sum_{j=i+1}^{N} \mathbf{f}_{\alpha,ij}[\theta(z_i - z)\theta(z - z_j) - \theta(z_j - z)\theta(z - z_i)]\right\rangle \quad (21)$$

When the force cannot be decomposed into pairwise contributions (PPPM method) and the system is periodic in all three directions, the use of the MOP methodology for the calculation of the pressure components is not possible.

5. Results and Discussion

5.1. Bulk Electrolyte. As a first test to validate the calculation of the pressure tensor, we consider the simple electrolyte previously studied by Groot[14] and Alejandre and co-workers.[15] The system consisted of $N = 3000$ particles in a simulation cell of volume $10 \times 10 \times 10$. The box contained 2804 neutral particles, 98 particles with a positive charge of $+e$ and 98 particles with a negative charge of $-e$. The total density number was $\rho = 3$. A typical configuration is shown in Figure 2a. Using the appropriate scaling given in Table C-1 of Appendix C, this system corresponds to a salt concentration of 0.6 M. The interaction parameters for the conservative, dissipative, and random forces were $a_{ij} = 25.0$, $\lambda = 4.5$, and $\sigma = 3.0$, respectively. The time step δt was equal to 0.02. Each simulation for these systems consisted of an equilibration period of 100 000 steps, followed by an acquisition period of 300 000 steps. The length of the production phase is about 1 μs. The periodic boundary conditions were applied in all three directions. Because the calculation of the pressure cannot be performed with a non-pairwise-additive force (PPPM method) in a three dimensionally periodic system, we can study only the 3D bulk electrolyte with the EW3DC method. We performed these simulations as a reference for the works described in section 5.3, where the box simulations represent the homogeneous phase in the middle of the cell.

Figure 3a shows the kinetic term for the pressure calculated according to the IK definition along the z direction in the bulk electrolyte. We observe that this profile is constant with a mean value of 3.11 ± 0.01. This corresponds to an average temperature of 0.99 ± 0.01, which agrees well with the input temperature of 1.0. This means that the incorporation of the electrostatic interactions allows for very accurate temperature control with the use of the velocity-Verlet algorithm and a time step of 0.02. Figure 3b represents the normal component of the configurational pressure tensor along the z direction calculated according to the IK and MOP approaches. As expected from a system mechanical equilibrium, the profile is constant, and the average pressure of p_{zz} calculated over the different z positions is equal to 20.7 ± 0.1 for the two definitions. The profiles of the real and reciprocal contributions of the Ewald summation method shown in Figure 3c are identical within the statistical fluctuations for the IK and MOP methods. The electrostatic contributions of -0.013 DPD units are relatively small compared to the magnitude of the configurational pressure. The value of pressure is determined from the contributions between ions of the same charge (0.11) and between ions of opposed charges (-0.123). The electrostatic interactions are small because of the strong cancellation between different ion pairs.

5.2. Electrolyte Embedded between Two Planar Surfaces. We now simulate the electrolyte between two planar solid surfaces composed of three layers of DPD particles tethered by springs to lattice points in a regular array (see Figure 2b for a typical configuration). Each surface was composed of a 17×18 layer of wall particles. The cell dimensions and the features of the system are given in Table 1. The separation distance between the two walls was 11. This value was chosen to reproduce a local value of the density number in the middle of the box similar to that of the bulk electrolyte system described in section 4.2. The time step was fixed at 0.02, and the simulations consisted of an

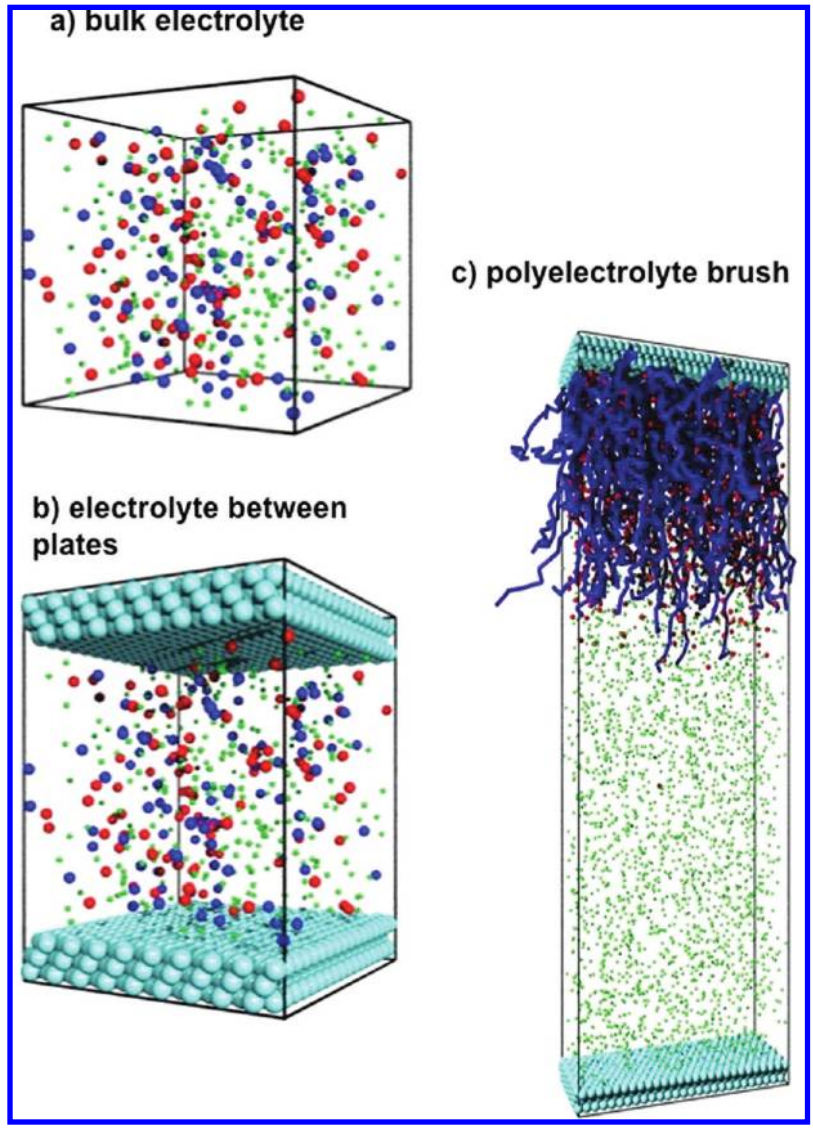

Figure 2. Typical configurations of the three simulated systems. The solvent particles, the anions or polymer beads, and the counterions are represented in green, blue, and red, respectively.

equilibration period of 100 000 steps, followed by an acquisition period of 300 000 steps. Periodic boundary conditions were applied in all three directions. The simulation box dimension was elongated in the z direction by adding an empty space of at least twice the space of the fluid-occupied region. We added a correction term to remove the forces due to the net dipole of the periodically repeating slabs.[17,23,24] The reciprocal vector $\mathbf{h}_z^{\max}$ was increased (see Table C-1 in Appendix C) to allow for the elongation of the cell in the z direction.

When the electrostatic interactions are calculated with EW3DC, the average value of the normal component of the configurational pressure calculated in the middle of the pore from the profiles of Figure 4a is 20.7 ± 0.1 for the IK and MOP methodologies. This value agrees very well with that calculated in the bulk electrolyte. Figure 4b shows the profiles of the real and reciprocal parts of the normal pressure components calculated from EW3DC. We observe flat profiles in the middle of the pore in agreement with a homogeneous distribution of the ions along this direction. From these profiles, we deduce an average value of -0.012 ± 0.001 in the center of the box for the total electrostatic pressure. This value matches reasonably well with that calculated (-0.013) by EW3DC in the bulk electrolyte system. This result validates the use of a local definition for the pressure calculation within the supercell approximation. Additionally, we find that the sum of the kinetic, configurational, and electrostatic contributions to the pressure tensor lead to a completely flat profile (not shown here) as expected for a system at mechanical equilibrium.

In addition, the profiles of the configurational pressure in Figure 4c calculated from simulations using the PPPM method are also in line with those resulting from the EW3DC technique. The electrostatic pressure calculated according to the PPPM method is slightly different from that coming from the EW3DC method, with an average difference of 6%. The profiles of the electrostatic contributions to the normal pressure are shown in Figure 4d. This difference in the pressure values can be attributed to the fact that the electrostatic force used in EW3DC is slightly different from that used in the PPPM method, as shown in Figure 1. However, from these profiles, we can conclude that the

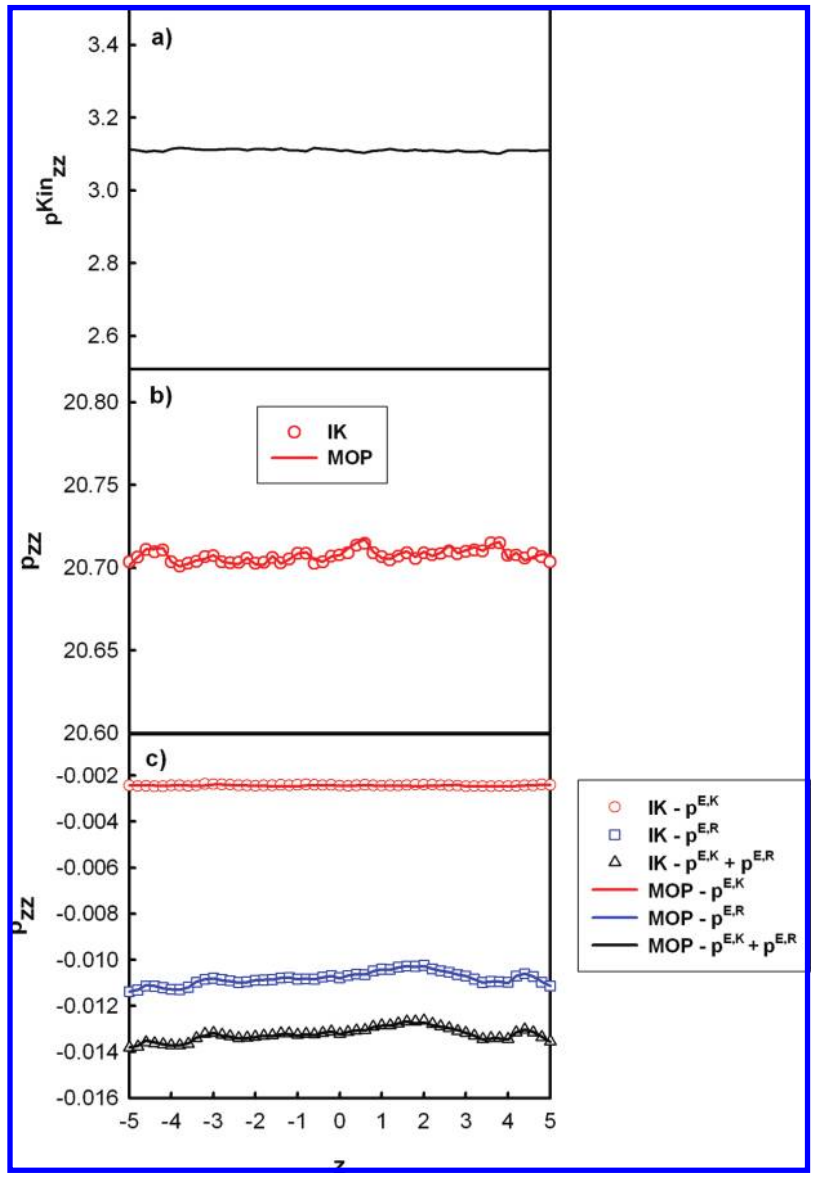

Figure 3. (a) Kinetic and (b) configurational pressure components along the normal to the surface for the bulk electrolyte system. Contributions of the normal component of the pressure tensor from the real ($p^{E,K}$) and reciprocal ($p^{E,R}$) spaces.

Table 1. Dimensions of the Box in Reduced Units and Number of Particles as a Function of the System

system	L_x/r_c	L_y/r_c	L_z/r_c	h	$N_{solvent}$	N_+[a]	N_-[a]
bulk electrolyte	10	10	10		2804	98	98
bulk electrolyte between surfaces	10.5	9.6	35	11	2804	98	98
polymer brush[b]							
f[c] = 0	16.7	6.4	152	50	13 863	0	0
f = 0.5	16.7	6.4	152	50	12 783	1080	0
f = 1.0	16.7	6.4	152	50	11 703	2160	0

[a] N_+ and N_- represent the numbers of cations and anions, respectively. [b] In a polyelectrolyte brush, the number of counterions N_+ is equal to fN_pN_b. [c] Charge fraction.

Table 2. Height of the Polymer Brush ($\langle z_m \rangle$), Height of the Counterion Layer ($\langle z_{ci} \rangle$), and Average Bond Length in the Polymer Chain ($\langle b \rangle$) Expressed in Reduced Units[a]

fraction of charge (f)	method	$\langle z_m \rangle$	$\langle z_{ci} \rangle$	$\langle b \rangle$
	Neutral Polymer Brush			
0		11.0		0.97
	Polyelectrolyte Brushes			
0.5	PPPM	15.1	16.0	1.05
0.5	EW3DC	15.1	16.1	1.06
1.0	PPPM	18.9	18.9	1.14
1.0	EW3DC	19.0	19.1	1.15

[a] Heights calculated from the first moment of the density profiles.

mechanical properties of the electrolytes between the two plates are very similar when they are calculated by EW3DC or by PPPM.

Parts a and b of Figure 5 show the two-dimensional radial distribution functions between solvent−solvent and equal and unequal ion pairs from simulations performed using the EW3DC and PPPM methodologies. These two-dimensional distribution functions were calculated in the middle of the cell in a slab of width 0.3. For each case, we include for comparison the three-dimensional pair correlation functions calculated in the bulk electrolytes. First, we observe that the two- and three-dimensional radial distribution functions are well-matched, indicating that the structure in the middle of

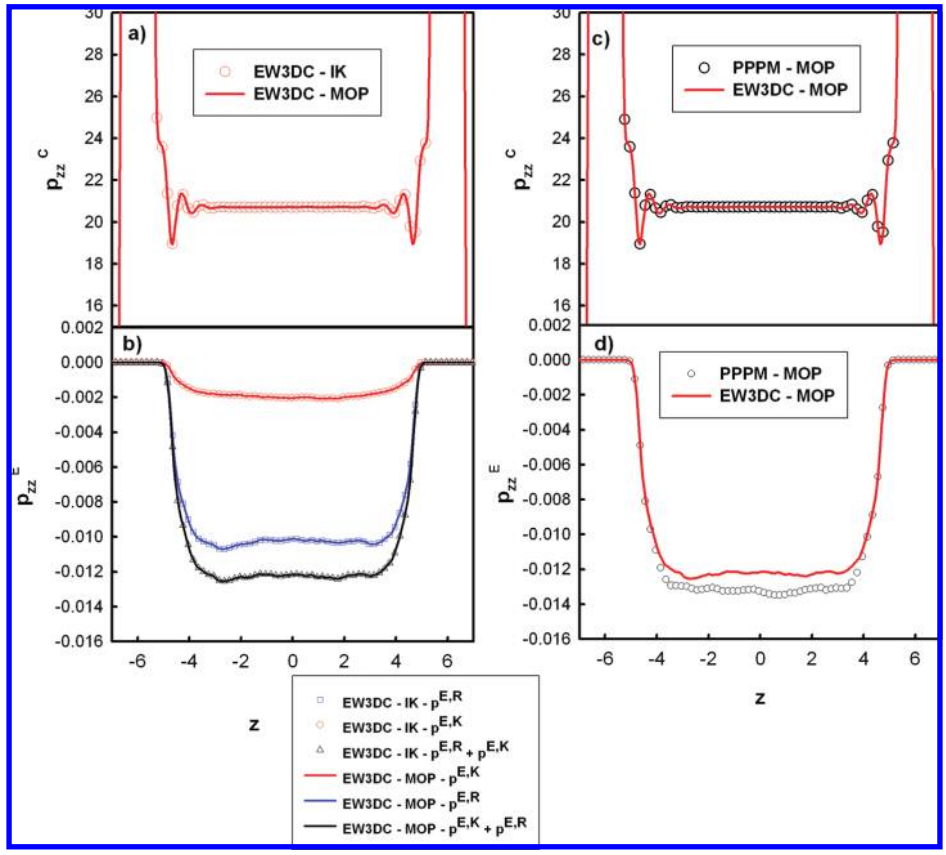

Figure 4. (a) Normal component (p^{C}_{zz}) of the configurational part of the pressure calculated according to the IK and MOP definitions using the EW3DC method, (b) normal component of the contributions of the real ($p^{E,K}$) and reciprocal ($p^{E,R}$) spaces calculated with the IK and MOP definitions using the EW3Dc method, (c) normal component (p^{C}_{zz}) of the configurational part of the pressure calculated with MOP using both the PPPM and EW3DC methods, and (d) total normal component of the electrostatic contribution calculated using the MOP definition within the EW3DC and PPPM methods. The system consisted of an electrolyte between two surfaces.

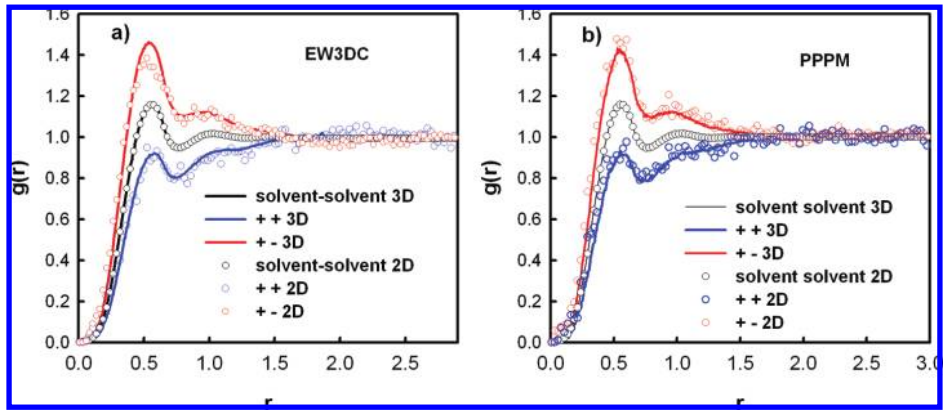

Figure 5. Two-dimensional and three-dimensional radial distribution functions for different ion pairs. The two-dimensional distribution functions were calculated in the middle of the box in a slab with a width of of $0.3r_c$, whereas the three-dimensional distribution functions were calculated in the bulk electrolyte.

the pore returns to that of the bulk. The two-dimensional curves are noisier because of the statistics. These distributions functions are also in line with those calculated in previous works by Alejandre and co-workers[15] and Groot.[14]

The calculation of the pressure components of the configurational and electrostatic parts in a system where a physical boundary prohibits passage of molecules in the third direction allows for the verification that the local definitions used for the pressure calculation (MOP and IK) are be relevant within the EW3DC and PPPM techniques. This was confirmed by comparing the structure and the mechanical properties of the central zone between the two surfaces with those of the three-dimensional bulk electrolytes.

This system allowed the relative speeds of the EW3DC and PPPM techniques to be compared. We simulated a confined polyelectrolyte of DPD particles between two walls. Initially, all of the particles were uncharged, and we performed a number of different simulations increasing the

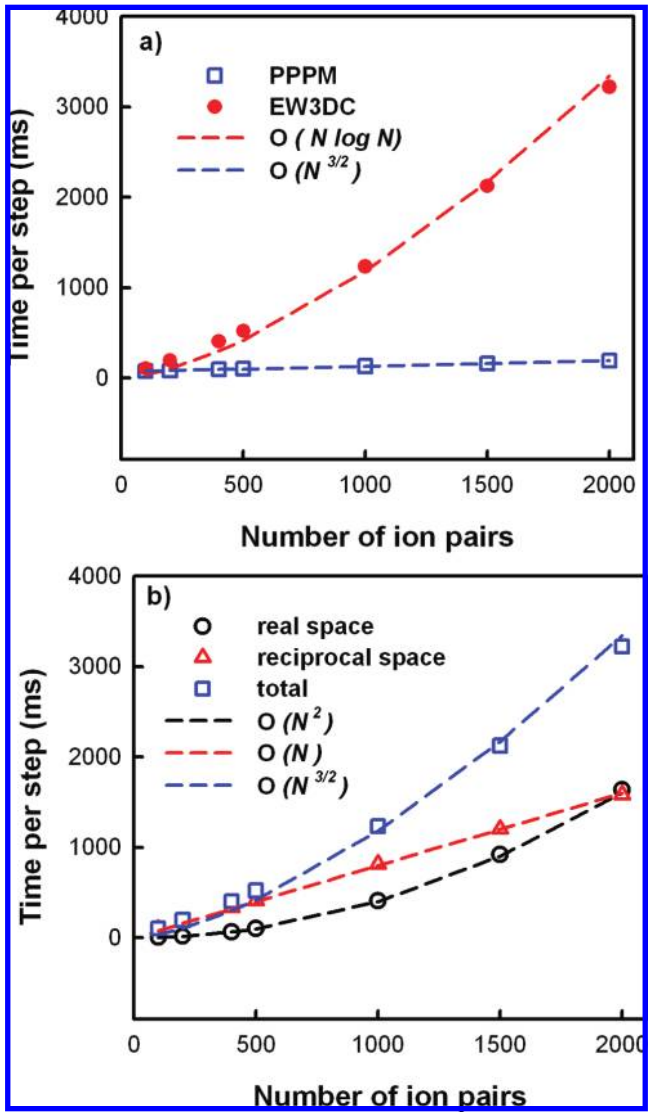

Figure 6. Run times (in milliseconds) for one time step (a) in the calculation of the electrostatic force and (b) in the calculation of the real- and reciprocal-space terms of the electrostatic force. The average time was calculated from a DPD simulation carried out over 10 000 steps. The total number of particles was fixed at 16 000. The number of ion pairs increased from 0 to 2000, and the number of solvent particles decreased from 16 000 to 12 000. The system was an electrolyte between two plates.

number N of ion pairs to 2000 while keeping the total number of particles fixed. Figure 6a shows the run time for one time step of a DPD simulation as a function of the number of ion pairs. The execution time for one time step includes only the calculation of the electrostatic force. This curve shows that the PPPM method becomes more efficient than EW3DC when the number of ion pairs is greater than 100. We verified that the EW3DC and PPPM methods scale as $O(N^{3/2})$[40] and $O(N \log N)$,[40] respectively. For the range of the number of ion pairs investigated here, the PPPM method performed faster than EW3DC for the study of polyelectrolytes with the DPD method. This is in line with Groot's observation[14] that the time used to distribute the charge, solve the field equation, and calculate the electrostatic forces is small compared to other elements of a time step. In Figure 6b, we show the times for the calculation of the reciprocal- and real-space terms of the electrostatic force in the EW3DC method. As expected from previous works,[40,41] the computation times for the calculation of the reciprocal- and real-space terms grow as N^2 and N, respectively. For the set of parameters (see Tables 1 and C-1) and numbers of ion pairs smaller than 1000, the computational cost of the calculation of the electrostatic forces with EW3DC comes from the calculation of the reciprocal-space term.

5.3. Polyelectrolyte Brushes. *5.3.1. Mechanical and Structural Properties.* Now that we have verified the consistency of the calculation of the local pressure within the supercell approximation in the EW3DC and PPPM methodologies, we focus on the calculation of the mechanical properties of a single polyelectrolyte brush. The system consisted of two planar solid surfaces composed of three layers of 324 DPD particles. The two surfaces were positioned at the top and bottom of the simulation cell. One of the two surfaces was coated with $N_p = 108$ polymer chains that were randomly grafted by a harmonic force acting between the end particles of the chains and the particles of the first layer of the wall. Each chain contained $N_b = 20$ polymer beads. The surface coverage was defined as $\rho_a = N_p/(L_xL_y)$. In our system, one-third of the wall particles of the third layer were connected to the first beads of the polymer chains. The different charge fractions f were 1 (completely negatively charged), 0.5 (half fully charged), and zero (neutral). To preserve electroneutrality, there are fN_pN_b counterions. The number of solvent particles was adjusted so that the overall reduced density between the two walls was close to 3. The cell dimensions are given in Table 1, and a representation of the simulation geometry is shown in Figure 2c. The a_{ij} parameters were set to 25 for all interactions. The polymer brush was then modeled in athermal solvent conditions. To respect the supercell approximation, the simulation cell was elongated along the z direction (see Table C-1 in Appendix C), and the reciprocal vector $\mathbf{h}_z^{max} = 17$ was changed accordingly. The time-step was fixed at 0.06, and the simulations consisted of an equilibration period of 100 000 steps, followed by an acquisition period of 300 000 steps.

Figure 7a shows the normal components of the total pressure calculated along the z direction according to the IK and MOP methods with the EW3DC methodology for the system with $f = 0.5$. Figure 7d compares the profiles of the total pressure calculated according to the MOP with EW3DC and PPPM. First, we found that the mechanical equilibrium is recovered for polyelectrolyte brushes with a very flat profile of the pressure across the simulation cell. This homogeneous profile of the normal component is independent of the method used for the pressure calculation and of the method used for the calculation of the long-range electrostatic interactions. Figure 7b shows the profiles of the normal component of the configurational (left axis) and electrostatic (right axis) pressure. Whereas the total pressure (left axis) exhibits a flat profile, one observes that the configurational part shows a positive contribution close to the grafted surface that is compensated by a symmetric negative value of the electrostatic pressure. One can observe

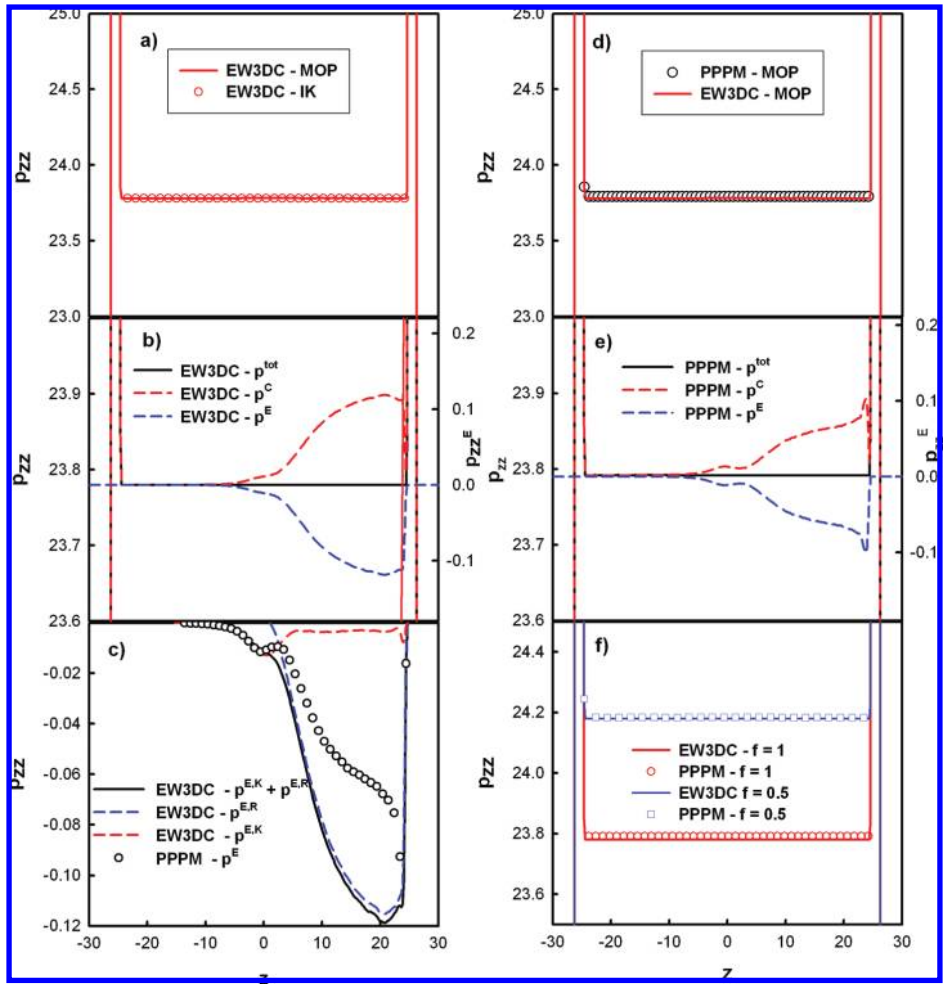

Figure 7. Normal component of the pressure (p_{zz}) as a function of the distance from the grafting surface calculated according to the MOP definition for (a) the total pressure calculated using EW3DC (included for comparison is the pressure profile calculated using IK); (b) the electrostatic (p^E), configurational (p^C), and total parts calculated using EW3DC; (c) the real-space ($p^{E,R}$) and reciprocal-space ($p^{E,K}$) contributions with the total electrostatic contribution calculated according to the EW3DC and PPPM methods; (d) the total pressure calculated using the EW3DC and PPPM methods; (e) the electrostatic (p^E), configurational (p^C), and total parts calculated using PPPM; and (f) the total pressure component for two different fractions of charges *f*. The configurational and total parts of the pressure in parts b and e are represented on the left axis, whereas the electrostatic pressure is represented on the right axis.

the same features with the PPPM methodology with slightly different profile shapes. The total pressures calculated by EW3DC and PPPM are identical. Figure 7c shows the profiles of the electrostatic pressure obtained by separating the real and reciprocal parts with the EW3DC method. The total electrostatic pressure is then compared to that calculated with the PPPM method. The slight differences between the pressure profiles obtained with EW3DC and PPPM are due to the fact that the force used with EW3DC is shifted to smaller distances compared to that used with PPPM (see Figure 1). Figure 7f shows that the total pressure decreases as the fraction of charges changes from 1 to 0.5.

Figure 8a shows the monomer density profiles $\rho_m(z)$ as a function of the distance from the grafting surface for three different fractions of charges (neutral, half-charged, and fully charged). First, we distinguish no difference in the density profiles obtained by the EW3DC and PPPM methods. We observe that, when the fraction of charge is increasing, the brush extends farther in the direction normal to the surface, although the profile remains parabolic. The electrostatic contribution to the pressure is relatively small compared to that of the configurational part, as the presence of the electrostatic interactions induces a strong stretching of the chains in the z direction. The repulsive electrostatic interactions between polymer chains and between beads within the chains tend to swell the brush and to straighten the polymer chain, respectively. These effects are lessened by the counterions that act to screen the charged monomer interactions. The decomposition of the electrostatic pressure into monomer−monomer, counterion−counterion, and monomer−counterion contributions yields values of 0.831, 0.836, and −1.691, respectively, for $f = 0.5$ and 2.717, 2.720, and −5.482, respectively, for $f = 1.0$. The resulting total electrostatic pressure within the brush is then equal to −0.024 for $f = 0.5$ and −0.045 for $f = 1.0$ in reduced units. This calculation shows the ability of the counterion to screen the charged monomer interactions. However, the reduction in entropy due to the presence of counterions in a small volume occupied by the polymer chains must be compensated by extending the chains against their elasticity. The competition

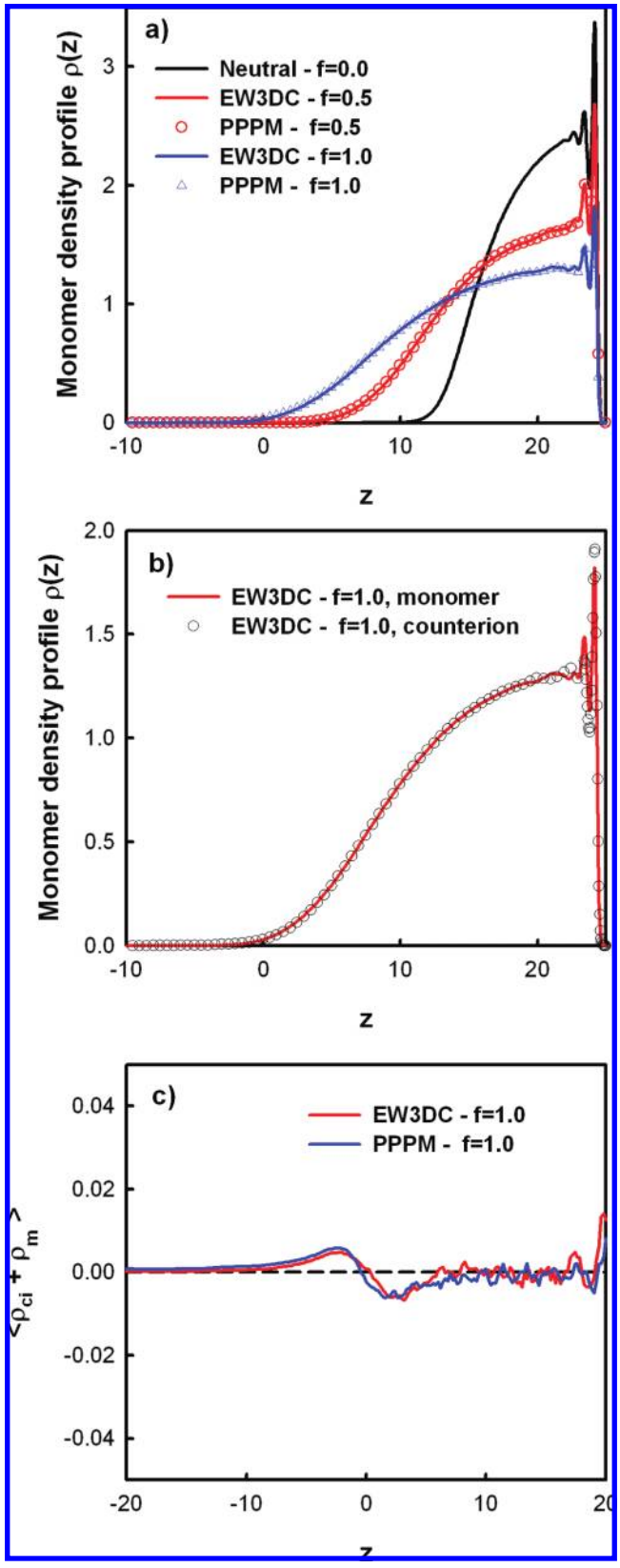

Figure 8. Monomer density profiles of the single polyelectrolyte brush calculated with different degrees of charged monomers.

among the entropy, Coulomb interactions, and chain elasticity is complex and is difficult to consider analytically in the theoretical predictions of polylectrolytes properties. To measure the extension of the brush, we calculated the average heights of the brush $\langle z_m \rangle$ and of the counterion layer $\langle z_{ci} \rangle$ from the first moment of the density profiles of monomers and counterions as

$$\langle z_m \rangle = 2\frac{\int_0^\infty z\rho_m(z)\,dz}{\int_0^\infty \rho_m(z)\,dz} \quad \text{and} \quad \langle z_{ci} \rangle = 2\frac{\int_0^\infty z\rho_{ci}(z)\,dz}{\int_0^\infty \rho_{ci}(z)\,dz} \tag{22}$$

where $\rho_m(z)$ and $\rho_{ci}(z)$ are the density profiles of the monolayer and the counterions, respectively. The factor of 2 takes into account the fact that the brush height is twice the first moment when the monomer density profile is uniform inside the brush. The different brush heights are reported in Table 2, along with the average distance $\langle b \rangle$ between neighboring beads within the polymer chain. This table highlights that the brush height is increased by 40% and 70% with respect to that of a neutral brush when the fractions of charges are 0.5 and 1.0, respectively. This elongation of the chain is reflected in part in the increase of the bond length in the polymer chain. This is allowed in part because of the soft potential used for the bond between neighboring beads (see eq 6). For the fully charged polymer chains, a brush height of 19 indicates that the chains are stretched to about 86% of their contour length defined from the limiting value for $N_b\langle b \rangle$ of 22 for a fully extended chain structure.

Part b of Figure 8 shows the density profiles of the polymer beads and the counterions. Interestingly, this figure emphasizes that the profile of the polymer beads is coincident with that of the counterions. This indicates that the counterions are mostly confined in the brush layer. The thickness of the layer of the counterions calculated from the first moment of the density profiles is listed in Table 2. As expected from the density profiles, the height of the counterion layer is very close to the brush height. It then becomes important to check the local electroneutrality across the brush by plotting the sum of the charges of the counterions and the polymer beads along the z direction. We note that the local eletroneutrality is satisfied in the direction perpendicular to the surface over almost the total brush height with two exceptions. The first relates to the local charge for $z > 20$ due to the layering of the grafted monomers close to the surface. The region close to the surface is not shown in part c of Figure 8. We also observe in the region close to the ends of the grafted chains a depletion of counterions with a negative local net charge, followed by a zone rich in counterions with a positive local charge. This leads to the formation of a local dipole. This has already been observed in the simulation of polyelectrolytes.[30,42] We also note that the electric properties in the brush layer are reproduced in the same way with the EW3DC and PPPM methodologies.

Figure 9a depicts the polyelectrolyte−ion pair distribution $p(r)$, where r corresponds to the separation distance between the ion and the closest polyelectrolyte bead. The distributions are normalized according to $2\pi\int_0^\infty rp(r)\,dr = 1$. This figure shows that these distributions are centered around 0.6 and 0.7 when the degree of charge decreases from 1.0 to 0.5. When the polymer chains are fully charged, the electrostatic interactions are stronger, and the

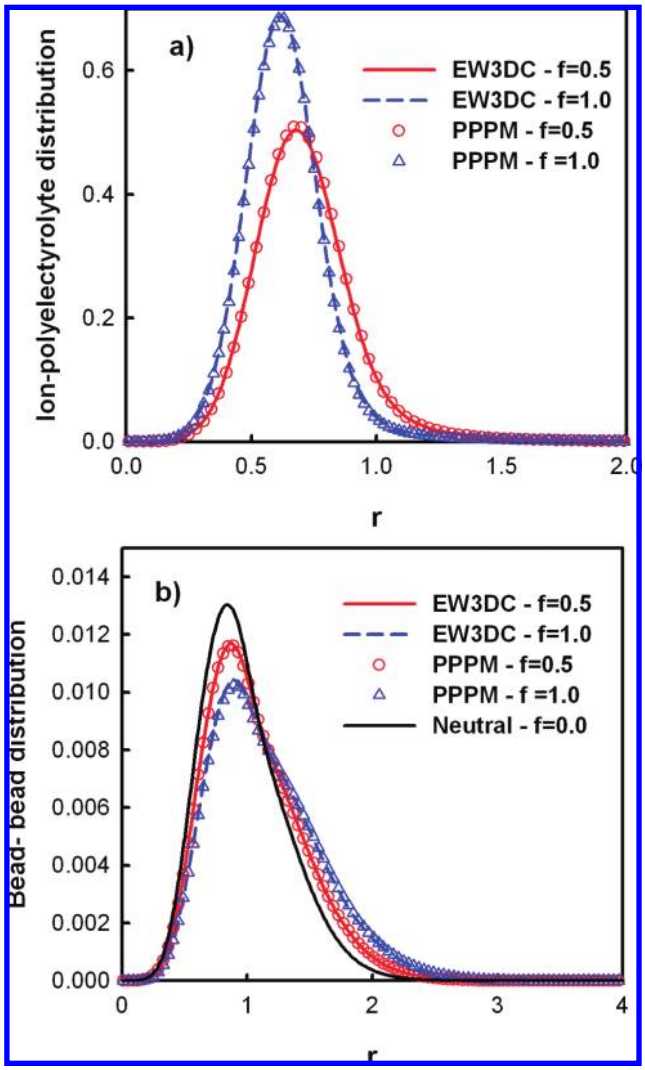

Figure 9. (a) Ion−polyelectrolyte distribution function calculated according to the EW3DC and PPPM methods for a fully charged polymer chain and a half-charged polymer chain, where *r* is the separation distance between polyelectrolyte bond and counterion, and (b) bead−bead distribution function between connected beads within the polymer chain as a function of the separation distance.

counterions are further trapped inside the chains to screen the charged monomer interactions. The resulting bead−counterion separation distance is then reduced. This figure also shows that there is a strong correlation between polyelectrolyte beads and counterions. The result is an inhomogeneous distribution of the counterions and contrasts with Pincus' theory,[43] which assumes that counterions form an ideal gas. Part b of Figure 9 shows the distribution of the distance between neighboring beads in the polymer chains and confirms the fact that the average bond length increases with the strength of the Coulomb interactions. These two structural properties illustrate that the entropic pressure of the confined counterions stretches the chains against their elasticity.

5.3.2. Scaling Properties. The basic behavior of polyelectrolyte brushes can be understood on the basis of simple scaling theory. This rationalization through the use of simple scaling arguments is sometimes useful, but the approximations used (shape of the monomer density profiles, strength of the electrostatic interactions, etc.) have not been validated by molecular simulation or experiment. The Bjerrum length, given by $\lambda_B = e^2/(4\pi k_B T \varepsilon_0 \varepsilon_r)$, characterizes the length scale at which the electrostatic interaction is equal to the thermal energy $k_B T$. According to the parameters used in this work, the Bjerrum length is equal to $1.11 \equiv 7.16$ Å. The dimensionless Manning ratio[44−46] is defined as $\lambda_B/\langle b \rangle$, where $\langle b \rangle$ is the average bond length distance between beads in the polyelectrolyte chain. In Manning's theory, the condensation of counterions occurs at $\lambda_B/\langle b \rangle = 1$. The values calculated for the bond length lead to values of the Manning ratio very close to 1 and are in line with the counterion condensation observed in our simulations. The degree of condensed counterions can be estimated from Figure 9a by assuming them to be condensed if the polyion−counterion distance is smaller than λ_B. This counterion condensation is 97% with $f = 0.5$ and $f = 1$. The Debye screening length associated with the counterions is defined as $\lambda_D = 1/(4\pi\lambda_B c_{ci})^{1/2}$, where c_{ci} can be estimated from the average density of counterions inside the brush. This parameter, defining the scale over which mobile charges are screened, is equal to 0.25 and 0.32 when the charge fraction is 0.5 and 1.0, respectively. This value, which is smaller than the bond length, explains in part why the counterions are trapped in the brush layer. Within the range of parameters used, the simulated brush is in the strong-charging and strong-streching limits. As a consequence, the model of polyelectrolyte brushes used follows the nonlinear osmotic brush regime.[47] This regime[47] combines the high-streching (nonlinear) version of the chain elasticity with the nonlinear entropic effects of the counterions inside the brush. This is also the case for previous molecular simulations of strongly charged polyelectrolyte brushes.[30,31,42,48]

Another typical length in the theory of polyelectrolyte brushes is the Gouy−Chapman length, λ_{GC}, defined as $1/(2\pi\lambda_B N_b f \rho_a)$, where N_b and ρ_a are the polymer chain length and the grafting density, respectively. This length defines the height at which counterions are effectively bound to a surface of charge density of $efN_b\rho_a$.[43] For a fully charged brush and a strong grafting density, the Gouy−Chapman length is on the order of $0.015 \equiv 0.1$ Å and can increase up to $0.015 \equiv 0.1$ Å for higher grafting densities. Within the nonlinear osmotic brush regime, the height of the counterion layer H is equal to the brush height plus $3\lambda_{GC}/2$. The weak values of λ_{GC} mean that the height of the brush is the same as that of a counterion layer with a high concentration of counterions inside the brush. It will be very interesting to investigate the dependence of the brush height on the grafting density within this regime, but we will consider this in a future work.

6. Conclusions

We have performed mesoscale modeling of different electrolyte systems: a bulk electrolyte, an electrolyte embedded between two surfaces, and a single polyelec-

trolyte brush. We have used the dissipative particle dynamics method to capture the physics of these complex systems at length and time scales that are outside the ranges of standard molecular simulations. Two methods were established recently for the calculation of the electrostatic interactions in the DPD formalism. The first method, initially introduced by Groot,[14] is an adaptation of the particle−particle particle-mesh (PPPM) method. The second method, initially developed by Alejandre and coworkers,[15] consists of using the standard Ewald summation method with charge distributions on particles to avoid the formation of artificial ion pairs (EW3DC).

We used the supercell approximation to allow the use of the three-dimensional EW3DC and PPPM methods in systems presenting a finite length along a given direction. We used two different definitions for the calculation of the local pressure. The Irving and Kirkwood definition is well-adapted for pairwise-additive forces and can be straitforwardly used with the EW3DC method. The PPPM method does not give a non-pairwise-additive electrostatic force, and the calculation of the local pressure in this method can be performed with the method of planes (MOP). We showed that the different techniques EW3DC and PPPM give similar profiles for the normal component of the pressure tensor for the configurational and electrostatic contributions. We also showed that the use of the supercell approximation with appropriate definitions of the pressure tensor allows for the calculation of the local pressure in agreement with that expected from a bulk electrolyte at the same density.

The calculation of the local pressure in a single polyelectrolyte brush demonstrated a positive configurational contribution to the pressure from the brush and a similar negative electrostatic part from the brush. The profile of the total pressure along the direction normal to the surface is flat, as expected for a system at mechanical equilibrium. We completed the study of the polyelectrolyte brush by calculating the heights of the brush and the counterion layer. We found that the counterions are mostly trapped in the brush and that the condensation of counterions increases with the fraction of charged monomers. The stretching of the polymer chain was found to about 85% of its contour length. These results were expected from the values of the dimensionless Manning ratio and the Debye screening length of the counterions. The weak value of the Gouy−Chapman length indicates that the height of the polymer brush must be equal to that of the counterion layer. The system model simulated here is in the strong-charging and strong-stretching limits and follows the nonlinear osmotic brush regime.

We also showed that the incorporation of the electrostatic interactions through the EW3DC and PPPM methods into the DPD methodology allows the main properties of a single strongly stretched polyelectrolyte brush made of strongly charged polymers to be recovered. This preliminary study calls for further investigation of the dependence of the brush height on the surface coverage, fraction of charge, and salt concentration. It is also interesting to see that an accurate calculation of the local pressure can be carried out in such systems at a mesoscopic scale. This represents an important step for the next calculation of the frictional forces in polyelectrolyte brushes under shear.

Additionally, the PPPM method is more efficient in CPU time than the EW3DC method as the number of charges increases. This makes the PPPM method a powerful and attractive method for the mesoscale modeling of polyelectrolytes.

Acknowledgment. The authors acknowledge A. Ghoufi, M. Gonzales-Melchor, F. Goujon, and R. D. Groot for helpful discussions.

Appendix A. Expression of the Electrostatic Potential in the DPD Method with the PPPM and EW3DC Techniques

The empirical expressions of the electrostatic potential used in the PPPM method[14] are given by

$$\frac{4\pi r_e U(r)}{\Gamma r_c} = \begin{cases} \frac{52}{35} - \frac{4}{5}\left(\frac{rr_c}{r_e}\right)^2 + \frac{2}{5}\left(\frac{rr_c}{r_e}\right)^4 - 0.13587\left(\frac{rr_c}{r_e}\right)^{5.145} & (r < r_e/r_c) \\ \frac{r_e}{rr_c} - 3.2100\left(1 - \frac{rr_c}{2r_e}\right)^6 & (r_e/r_c < r < 2r_e/r_c) \\ \frac{rr_c}{r_e} & (r < r_e/r_c) \end{cases} \quad \text{(A-1)}$$

The potential and the corresponding force are represented in Figure 1.

The electrostatic potential used in the DPD method with the EW3DC technique[15] is given by

$$\frac{4\pi r_e U(r)}{\Gamma r_c} = \frac{1}{r}[1 - (1 + \beta r)\exp(-2\beta r)] \quad \text{(A-2)}$$

and its corresponding force is given by

$$\frac{4\pi r_e^2 f(r)}{\Gamma r_c^2} = \frac{1}{r^2}\{1 - \exp(-2\beta r)[1 + 2\beta r(1 + \beta r)]\} \quad \text{(A-3)}$$

The expressions for the energy and forces are represented in Figure 1 for comparison with those used in the PPPM method.

Appendix B. Calculation of the Electrostatic Contributions to the Pressure of the EW3DC Method with the IK and Harasima Definitions

The contribution of the real space to the local pressure is given by

$$p_{\alpha\beta}^{E,R}(z) = \frac{\Gamma}{4\pi}\left\langle \sum_{i=1}^{N-1}\sum_{j=i+1}^{N} q_i q_j \left[\frac{2}{\sqrt{\pi}}\alpha r_{ij}\exp(-\alpha^2 r_{ij}^2) + \operatorname{erfc}(\alpha r_{ij})\right]\frac{(\mathbf{r}_{ij})_\alpha \cdot (\mathbf{r}_{ij})_\beta}{r_{ij}^3}\frac{1}{|z_{ij}|}\theta\left(\frac{z - z_i}{z_{ij}}\right)\theta\left(\frac{z_j - z}{z_{ij}}\right)\right\rangle \quad \text{(B-1)}$$

Table C-1. DPD Parameters in Reduced Units, along with Some Typical Parameters in Real Units

parameter	DPD value	real units	definition
		DPD	
a_{ij}	25	1.59×10^{-19} J m^{-1}	repulsion parameter between particles *i* and *j*
T	1	298 K	temperature
m	1	8.97×10^{-27} kg	particle mass
N_m		3	number of water molecules within one bead
r_c	1	6.4633 Å	range of repulsive interaction
ρ	3	1.0 g cm^{-3}	density
δt	0.02−0.06	3.2−9.6 ps	time step
τ	1	160 ps	time scale
σ	3	2.92×10^{-11} J m^{-1} s$^{1/2}$	noise amplitude
γ	4.5	1.04×10^{-1} J m^{-2} s	friction coefficient
v	1.0	4.04 m s^{-1}	velocity
p	1.0	15.22 MPa	pressure
r_e	1.6	10.34 Å	range over which charges are smeared
		DPD + EW3DC	
α	0.9695	0.15 Å^{-1}	Ewald convergence factor
r_c^R	3.0	19.39 Å	electrostatic cutoff for the real part
$\mathbf{h}_x^{max} = 5$	$\mathbf{h}_y^{max} = 5$	$\mathbf{h}_z^{max} = 5$	bulk electrolyte
$\mathbf{h}_x^{max} = 5$	$\mathbf{h}_y^{max} = 5$	$\mathbf{h}_z^{max} = 17$	bulk electrolyte between two surfaces
$\mathbf{h}_x^{max} = 8$	$\mathbf{h}_y^{max} = 3$	$\mathbf{h}_z^{max} = 76$	single polyelectrolyte brush

and that of the reciprocal space is given by

$$p_{\alpha\beta}^{E,K}(z) = \frac{\Gamma}{4\pi}\left\langle \frac{2\pi}{V^2}\sum_{\mathbf{h}\neq 0} H(z_i)\, Q(h)\, S(\mathbf{h})\, S(-\mathbf{h}) \times \left(\delta_{\alpha\beta} - \frac{2\mathbf{h}_\alpha \mathbf{h}_\beta}{h^2} - \frac{\mathbf{h}_\alpha \mathbf{h}_\beta}{2\alpha^2}\right)\right\rangle \quad \text{(B-2)}$$

where $H(z_i)$ is a top-hat function defined as

$$H(z_i) = \begin{cases} 1 & \text{if } z - \Delta z/2 < z_i < z + \Delta z/2 \\ 0 & \text{otherwise} \end{cases} \quad \text{(B-3)}$$

Appendix C. DPD Parameters, Physical Length, and Time Scales

In the simulations, the particle mass, temperature, and interaction range were chosen as units of mass, energy, and length, respectively; hence $m = k_B T = r_c = 1$. The unit of time, τ, then becomes $r_c(m/k_B T)^{1/2}$. The real length r_c can be estimated from the volume of a DPD bead. If N_m represents the number of water molecules within a DPD particle, then $r_c = (\rho^* N_m V_m / N_A)^{1/3}$, where ρ^* is the reduced density of DPD particles, $V_m = 18$ cm ^{3} mol^{-1}, and N_A is Avogadro's number. Groot and Rabone[8] and Groot[14] used $N_m = 3$ and a reduced density of 3. Using such values, $r_c = 6.46$ Å. Making the Poisson equation dimensionless[14] implies that the coupling constant Γ is given by $e^2/(k_B T \varepsilon_0 \varepsilon_r r_c)$, where e is the electron charge, $\varepsilon_0 = 8.85418782 \times 10^{-12}$ C^2 J^{-1} m^{-1} is the dielectric constant of a vacuum, and $\varepsilon_r = 78.3$ is the relative permittivity of water at 298 K. Using $r_c = 6.46$ Å and $\Gamma = 13.87$, to match the interaction between two charge clouds at $r = 0$ within the PPPM and EW3DC methodologies, the β parameter is 0.929.[15] As already dicussed by Groot and Rabone,[8] the time scale is fixed by matching the diffusion constant of water. For the repulsion parameter $a = 25$, we found that the natural unit of time τ is 160 ps.

The complete list of DPD parameters in reduced units is provided in Table C-1.

References

(1) Hoogerbrugge, P. J.; Koelman, J. M. V. A. *Europhys. Lett.* **1992**, *19*, 155.

(2) Koelman, J. M. V. A.; Hoogerbrugge, P. J. *Europhys. Lett.* **1993**, *21*, 363.

(3) Espanol, P.; Warren, P. B. *Europhys. Lett.* **1995**, *30*, 191.

(4) Espanol, P. *Europhys. Lett.* **1997**, *40*, 631.

(5) Groot, R. D.; Madden, T. J. *J. Chem. Phys.* **1998**, *108*, 8713.

(6) Groot, R. D.; Madden, T. J.; Tildesley, D. J. *J. Chem. Phys.* **1999**, *110*, 9739.

(7) Groot, R. D. *Langmuir* **2000**, *16*, 7493.

(8) Groot, R. D.; Rabone, K. L. *Biophys. J.* **2001**, *81*, 725.

(9) Malfreyt, P.; Tildesley, D. J. *Langmuir* **2000**, *16*, 4732.

(10) Irfachsyad, D.; Tildesley, D. J.; Malfreyt, P. *Phys. Chem. Chem. Phys.* **2002**, *4*, 3008.

(11) Goujon, F.; Malfreyt, P.; Tildesley, D. J. *ChemPhysChem* **2004**, *5*, 100.

(12) Goujon, F.; Malfreyt, P.; Tildesley, D. J. *Mol. Phys.* **2005**, *103*, 2675.

(13) Raviv, U.; Giasson, S.; Kampf, N.; Gohy, J. F.; Jerome, R.; Klein, J. *Nature* **2003**, *425*, 163.

(14) Groot, R. D. *J. Chem. Phys.* **2003**, *118*, 11265.

(15) Gonzalez-Melchor, M.; Mayoral, E.; Velazquez, M. E.; Alejandre, J. *J. Chem. Phys.* **2006**, *125*, 224107/1.

(16) Ewald, P. P. *Ann. Phys.* **1921**, *64*, 253.

(17) Goujon, F.; Malfreyt, P.; J. Tildesley, D. *J. Chem. Phys.* **2008**, *129*, 034902.

(18) Irving, J. H.; Kirkwood, J. G. *J. Chem. Phys.* **1950**, *18*, 817.

(19) Harasima, A. *Adv. Chem. Phys.* **1958**, *1*, 203.

(20) Alejandre, J.; Tildesley, D. J.; Chapela, G. A. *J. Chem. Phys.* **1995**, *102*, 4574.

(21) Sonne, J.; Hansen, F. Y.; Peters, G. H. *J. Chem. Phys.* **2005**, *122*, 124903.

(22) Todd, B. D.; Evans, D. J.; Daivis, P. J. *Phys. Rev. E* **1995**, *52*, 1627.

(23) Yeh, I. C.; Berkowitz, M. L. *J. Chem. Phys.* **1999**, *111*, 3155.

(24) Crozier, P. S.; Rowley, R. L.; Spohr, E.; Henderson, D. *J. Chem. Phys.* **2000**, *112*, 9253.

(25) Goujon, F.; Bonal, C.; Limoges, B.; Malfreyt, P. *Mol. Phys.* **2008**, *106*, 1397.

(26) Hautman, J.; Klein, M. *Mol. Phys.* **1992**, *75*, 379.

(27) Lekner, J. *Physica A* **1991**, *176*, 485.

(28) Strebel, R.; Sperb, R. *Mol. Simul.* **2001**, *27*, 61.

(29) Arnold, A.; Holm, C. *Comput. Phys. Commun.* **2002**, *148*, 327.

(30) Kumar, N. A.; Seidel, C. *Macromolecules* **2005**, *38*, 9341.

(31) Kumar, N. A.; Seidel, C. *Phys. Rev. E* **2007**, *76*, 020801.

(32) Beckers, J. V. L.; Lowe, C. P.; de Leeuw, S. *Mol. Simul.* **1998**, *20*, 368.

(33) Deserno, M.; Holm, C. *J. Chem. Phys.* **1998**, *109*, 7678.

(34) Sagui, C.; Darden, T. *J. Chem. Phys.* **2001**, *114*, 6578.

(35) Eastwood, J. W.; Hockney, R. W.; Lauwrence, D. *Comput. Phys. Commun.* **1980**, *19*, 215.

(36) Smith, E. R. *Proc. R. Soc. London, Ser. A* **1981**, *375*, 475.

(37) Rowlinson, J. S.; Widom, B. *Molecular Theory of Capillarity*; Clarendon Press: Oxford, U.K., 1982.

(38) Walton, J. P. R. B.; Tildesley, D. J.; Rowlinson, J. S.; Henderson, J. R. *Mol. Phys.* **1983**, *48*, 1357.

(39) Walton, J. P. R. B.; Tildesley, D. J.; Rowlinson, J. S. *Mol. Phys.* **1986**, *58*, 1013.

(40) Toukmaji, A. Y.; Board, J. A., Jr. *Comput. Phys. Commun.* **1996**, *95*, 73.

(41) Perram, J.; Petersen, H.; Leeuw, S. D. *Mol. Phys.* **1988**, *65*, 875.

(42) Csajka, F. S.; Seidel, C. *Macromolecules* **2000**, *33*, 2728.

(43) Pincus, P. *Macromolecules* **1991**, *24*, 2912.

(44) Manning, G. S. *Biophys. Chem.* **1977**, *7*, 95.

(45) Manning, G. S. *Q. Rev. Biophys.* **1978**, *11*, 179.

(46) Heath, P. J.; Schurr, J. M. *Macromolecules* **1992**, *25,* 4149.

(47) Ahrens, H.; Förster, S.; Helm, C. A.; Kumar, N. A.; Naji, A.; Netz, R. R.; Seidel, C. *J. Phys. Chem. B* **2004**, *108*, 16870.

(48) Seidel, C. *Macromolecules* **2003**, *36*, 2536.

CT900296S